# Structural, EPR, and Electrochemical Studies of Binuclear Copper(II) Complexes of Bis(pentadentate) Ligands Derived from Bis(1,4,7-triazacyclonane) Macrocycles

**Suzanne J. Brudenell,[†] Leone Spiccia,*[,†] Alan M. Bond,[†] Peter Comba,[‡] and David C. R. Hockless[§]**

Department of Chemistry, Monash University, Clayton, Victoria 3168, Australia, Anorganisch-Chemisches Institut, University of Heidelberg, Im Neuenheimer Feld 270, 69120, Heidelberg, Germany, and Research School of Chemistry, Australian National University, Canberra ACT 2601, Australia

*Received December 30, 1997*

Structural, electrochemical, and EPR studies of binuclear copper(II) complexes of bis(pentadentate) ligands, obtained by attaching 2-pyridylmethyl arms to the four secondary nitrogens of bis(tacn) macrocycles linked by ethyl (tmpdtne, $[Cu_2(tmpdtne)](ClO_4)_4 \cdot 2H_2O$ **2**), propyl (tmpdtnp, $[Cu_2(tmpdtnp)](ClO_4)_4$ **3**), butyl (tmpdtnb, $[Cu_2(tmpdtnb)](ClO_4)_4$ **4**), *m*-xylyl (tmpdtn*m*-X, $[Cu_2(tmpdtnm\text{-}X)](ClO_4)_4 \cdot 2DMSO \cdot 2H_2O$, **5**), and 2-propanol (tmpdtnp-OH, $[Cu_2(tmpdtnp\text{-}OH)](ClO_4)_4 \cdot 2H_2O$, **6**) bridges, are reported, together with further analysis of the mononuclear complex, $[Cu(dmptacn)](ClO_4)_2$ **1**, dmptacn = 1,4-bis(2-pyridylmethyl)-1,4,7-triazacyclononane. Single-crystal X-ray diffraction studies established the molecular structure of **3** and the tetrakis(DMF) solvate of **4**. Complex **3** crystallizes in the monoclinic space group $P2_1/c$ (No. 14) with $a = 13.867(3)$, $b = 13.548(6)$, $c = 28.055(4)$ Å, $\beta = 102.63(1)°$, $V = 5143(2)$ Å$^3$, and $Z = 4$. Refinement gave $R = 0.085$ and $R_w = 0.089$ for 3696 observed reflections. **4** crystallizes in the triclinic space group $\bar{P}$ (No. 2) with $a = 11.775(4)$, $b = 12.718(3)$, $c = 13.201(3)$ Å, $\alpha = 61.25(2)$, $\beta = 75.99(3)$, $\gamma = 77.66(3)°$, $V = 1673(1)$ Å$^3$, and $Z = 1$. Refinement gave $R = 0.072$ and $R_w = 0.065$ for 3876 observed reflections. In **4**, the pentadentate compartments are oriented in an anti configuration, while in **3**, constraints introduced by the propane bridging group result in a syn configuration. Both complexes exhibit distorted square pyramidal (SP) geometries about the Cu(II) centers with Cu−N(apical) ≈ 2.25 Å and Cu−N(equatorial) ≈ 2.0 Å. Molecular mechanics calculations have been carried out on these types of complexes for the first time in order to predict the solution structures of **5** and **6**. The calculations revealed that the SP geometry is also preferred by these complexes and that there is little energy difference between the syn and anti configurations. Cyclic, square-wave, and steady-state voltammetric studies on **1**−**6** indicate that, on the time scale of the measurements, **1** undergoes a one-electron reduction to the Cu(I) state while **2**−**6** undergo an overall two-electron reduction to the binuclear Cu(I) complexes. For **2**−**4**, a shift in reduction potential to more negative values with increasing Cu···Cu separation reflects the stabilization of the Cu(II) state while the two partially resolved reduction processes for **6** suggest that the alcohol group in the ligand backbone promotes a small level of interaction between copper centers.

## Introduction

In a recent publication,[1] we detailed the development of a series of bis(pentadentate) ligands obtained through the addition of 2-pyridylmethyl pendant arms to bis(tacn) ligands linked by ethyl (dtne),[2] propyl (dtnp),[2] and butyl (dtnb)[3] bridging groups (Chart 1). Bis(pentadentate) ligands of this type are rare, although ligands with alcohol[4] and acetate[5] pendant arms have been reported (Chart 2). For the pyridyl series (tmpdtne etc.), the coordination properties of the ligands were examined through the study of the copper(II) complexes but only the structure of the tmpdtne complex (Chart 1, **2**) was reported, owing to difficulties in obtaining crystals suitable for crystallography. Interestingly, in the structures of the Cu(II) complexes of such bis(pentadenate) ligands, the preferred orientation of the pentadenate compartments is anti rather than syn, with the exception of a Cu(II) complex of the dtne ligand bearing alcohol pendant arms.[4] In this particular case, the pendant arms stabilize the syn conformation through H-bonding following deprotonation of two of the pendant groups. In this paper, we report the X-ray structures of the copper(II) complexes of the tmpdtnp and tmpdtnb ligands (Chart 1, **3** and **4**) together with an examination of the ability of molecular mechanics combined with the simulation of ESR spectra to predict the solution structures of these complexes. The series of bis(pentadentate) ligands has been extended to include the 2-propanol (tmpdtnp-OH) and the *m*-xylyl (tmpdtn*m*-X) linked ligands by functionalization of the corresponding bis(tacn) macrocycles, viz., (dtnp-OH)[6] and

* Corresponding author.
† Monash University.
‡ University of Heidelberg.
§ Australian National University.

(1) Brudenell, S. J.; Spiccia, L.; Tiekink, E. R. T. *Inorg. Chem.* **1996**, *35*, 1975.
(2) Wieghardt, K.; Tolksdorf, I.; Herrmann, W. *Inorg. Chem.* **1985**, *24*, 1230.
(3) Sessler, J. L.; Sibert, J. W.; Lynch, V. *Inorg. Chem.* **1990**, *29*, 4143.
(4) Blake, A. J.; Donlevy, T. M.; England, P. A.; Fallis, I. A.; Parsons, S.; Schröder, M. *J. Chem. Soc., Chem. Commun.* **1994**, 1981.
(5) Fry, F. H.; Graham, B.; Spiccia, L.; Hockless, D. C. R.; Tiekink, E. R. T. *J. Chem. Soc., Dalton Trans.* **1997**, 827.
(6) Sessler, J. L.; Sibert, J. W.; Burrell, A. K.; Lynch, V. *Inorg. Chem.* **1993**, *32*, 4277.

S0020-1669(97)01634-0 CCC: $15.00 
Published on Web 07/01/1998

**Chart 1**

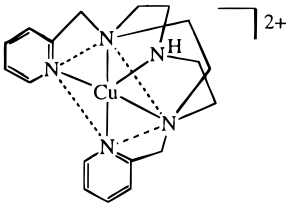

**1** $[Cu(dmptacn)]^{2+}$

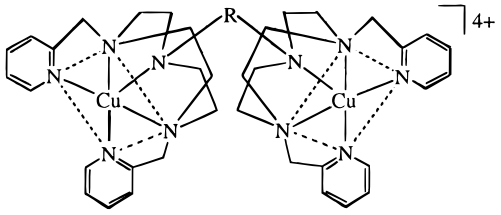

**2** $[Cu_2(tpdtne)]^{4+}$ R = $CH_2CH_2$

**3** $[Cu_2(tpdtnp)]^{4+}$ R = $CH_2CH_2CH_2$

**4** $[Cu_2(tpdtnb)]^{4+}$ R = $CH_2CH_2CH_2CH_2$

**5** $[Cu_2(tpdtn$*m*$\text{-X})]^{4+}$ R = *m*-xylyl

**6** $[Cu_2(tpdtnp\text{-}OH)]^{4+}$ R = $CH_2CH(OH)CH_2$

**Chart 2**

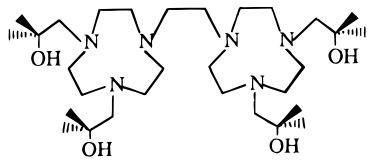

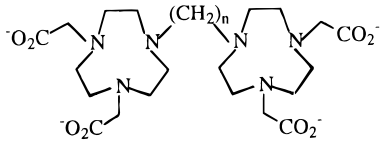

n = 2, 4

(dtn*m*-X).[7,8] These have been used to prepare Cu(II) complexes (Chart 1, **5**, and **6**), and in the absence of crystallographic data, force field calculations[9] coupled with comparisons of predicted and observed ESR spectra[10,11] are used to establish the most likely structure of these complexes. The systematic variation in the length and type of spacer in this series of complexes indicated that the complexes could have interesting electrochemical properties which could vary according to Cu···Cu separation and the type of spacer group. Consequently, a detailed investigation of the electrochemistry of these complexes and the mononuclear complex of dmptacn (Chart 1, **1**) was undertaken using cyclic voltammetry and square-wave voltammetry at a conventional Pt macrodisc electrode, near steady-state voltammetry at a Pt microdisk electrode, and bulk electrolysis at a Pt basket electrode.

## Experimental Section

**Materials and Reagents.** Reagent or AR grade materials were used throughout the study. The ligands 1,2-bis(1,4,7-triazacyclonon-1-yl)-ethane (dtne),[2] 1,3-bis(1,4,7-triazacyclonon-1-yl)propane (dtnp),[2] 1,4-bis(1,4,7-triazacyclonon-1-yl)butane (dtnb),[3] 1,3-bis(1,4,7-triazacyclonon-1-ylmethyl)benzene hexahydrobromide (dtn*m*-X·6HBr·1.5$H_2O$),[7,8] 1,2-bis[*N, N*′-bis(2-pyridylmethyl)-1,4,7-triazacyclonon-1-yl]ethane (tmpdtne),[1] 1,3-bis[*N,N*′-bis(2-pyridylmethyl)-1,4,7-triazacyclonon-1-yl]propane (tmpdtnp),[1] 1,4-bis[*N,N*′-bis(2-pyridylmethyl)-1,4,7-triazacyclonon-1-yl]butane (tmpdtnb),[1] and 1,4-bis(2-pyridylmethyl)-1,4,7-triazacyclononane (dmptacn)[12] were all prepared by published methods. The synthesis of 1,3-bis(1,4,7-triazacyclonon-1-yl)-2-hydroxypropane·6HBr was as detailed by Sessler et al.[6] with the exception that acid hydrolysis was carried out with concentrated sulfuric acid for 2 days at 90 °C rather than reductive detosylation with 2% Na amalgam. The yields achieved by the modified method were typically 80%. The Cu(II) complexes of dmptacn, $[Cu(dmptacn)](ClO_4)_2$ (**1**),[13] tmpdtne, $[Cu_2(tmpdtne)](ClO_4)_4\cdot 2H_2O$ (**2**),[1] tmpdtnp, $[Cu_2(tmpdtnp)](ClO_4)_4$ (**3**),[1] and tmpdtnb, $[Cu_2(tmpdtnb)](ClO_4)_4$ (**4**),[1] were prepared as described in our previous studies. Long, thin, blue-purple pleochroic crystals of **3** were grown by slow evaporation of a $CH_3CN/H_2O$ mixture, while small, square, blue crystals of tetrakis(DMF) solvate of **4** were grown from a mixture of $DMF/CH_3CN/H_2O$. These proved suitable for single-crystal X-ray crystallography.

**Caution!** *Although no problems were encountered in this work, transition metal perchlorates are potentially explosive. They should be prepared in small quantities and handled with care.*

**Physical Measurements.** $^1H$ and $^{13}C$ NMR spectra were recorded on a Bruker AC200 spectrometer with sodium 3-trimethylsilylpropionate as internal calibrant. Infrared spectra were measured on a Perkin-Elmer 1600 FTIR spectrometer as KBr pellets or Nujol mulls. Electronic spectra were recorded on either a Cary 3 or a Cary 5G spectrophotometer. Electron microprobe analyses were made with a Jeol JSM-1 scanning electron microscope through an NEC X-ray detector and pulse processing system connected to a Packard multichannel analyzer. Microanalyses were performed by Chemical and Micro-Analytical Services (CMAS) Melbourne, Australia. Copper determinations were carried out by EDTA titration with fast sulfon black F indicator.[14] Perchlorate content was determined gravimetrically as $Ph_4AsClO_4$. EPR spectra were measured on a Bruker ECS 106 spectrometer as frozen (99 K) DMF solutions using a concentration of 0.5 mM. Conductivity measurements were made using a Crison 522 conductimeter with Pt black electrodes. Standard KCl (0.020 M) with a conductivity of 2.77 mS $cm^{-1}$ was used as a calibrant. Room-temperature magnetic moments were determined by the Faraday method. Diamagnetic corrections were made using Pascal's constants. Low-temperature magnetic susceptibility measurements were carried out on a Quantum Design MPMS SQUID magnetometer as described previously.[12] Electrospray ionization mass spectra were recorded on either a Micromass Platform QMS with an electrospray source or a Bruker BioApex 47e FTMS with a 4−7 T superconducting magnet and an Analytica electrospray source.

Cyclic, square-wave, and steady-state voltammograms were recorded on a Cypress CS 1090 system. All measurements were made in dry, nitrogen-degassed acetonitrile solutions (~0.5 mM) with tetrabutylammonium perchlorate (0.1 M) as the supporting electrolyte. A platinum macrodisk working electrode ($r$ = 0.8 mm), a platinum auxiliary electrode, and a $Ag/Ag^+$ (10 mM $AgNO_3$) reference electrode were used to measure cyclic and square-wave voltammograms. Near steady-state voltammograms were measured in an aluminum Faraday cage using a platinum microelectrode ($r$ = 5 $\mu$m), a platinum auxiliary

(7) Farrugia, L. J.; Lovatt, P. A.; Peacock, R. D. *J. Chem. Soc., Dalton Trans.* **1997**, 911.
(8) Graham, B.; Fallon, G. D.; Hearn, M. T. W.; Hockless, D. C. R.; Lazarev, G.; Spiccia, L. *Inorg. Chem.* **1997**, *36*, 6366.
(9) Bernhardt, P. V.; Comba, P. *Inorg. Chem.* **1992**, *31*, 2638.
(10) Comba, P.; Hilfenhaus, P. *J. Chem. Soc., Dalton Trans.* **1995**, 3269.
(11) (a) Bernhardt, P. V.; Comba, P.; Hambley, T. W.; Massoud, S. S.; Stebler, S. *Inorg. Chem.* **1992**, *31*, 2644. (b) Comba, P.; Hambley, T. W.; Hilfenhaus, P.; Richens, D. T. *J. Chem. Soc., Dalton Trans.* **1996**, 533.
(12) McLachlan, G. A.; Fallon, G. D.; Martin, R. L.; Moubaraki, B.; Murray, K. S.; Spiccia, L. *Inorg. Chem.* **1994**, *33*, 4663.
(13) McLachlan, G. A.; Fallon, G. D.; Martin, R. L.; Spiccia, L. *Inorg. Chem.* **1995**, *34*, 254.
(14) Vogel, A. I. *Quantitative Inorganic Analysis* 4th ed.; Longman: London, 1978; p 321.

electrode, and a $Ag/Ag^+$ (10 mM $AgNO_3$) reference electrode using a scan rate of 10 $mVs^{-1}$. Potentials are reported relative to the ferrocene/ferrocinium ($F_c/F_c^+$) couple, which was used as an internal standard. Computer simulations of the CV data were performed using the DigiSim 2.1 software program.[15] The redox potentials ($E_{1/2}$ values) were determined from the cyclic voltammograms as the midpoint between the oxidation ($E_p^{ox}$) and reduction ($E_p^{red}$) potentials, $E_{1/2} = 1/2(E_p^{ox} + E_p^{red})$. Bulk electrolysis experiments were undertaken with a BAS100 electrochemical analyzer at a Pt basket electrode, using the same reference electrode as for voltammetry and a large Pt gauze auxiliary electrode separated from the test solution by a salt bridge.

**Syntheses. 1,3-Bis(*N,N′*-bis(2-pyridylmethyl)-1,4,7-triazacyclonon-1-ylmethyl)benzene (tmpdtn*m*-X) and 1,3-Bis[*N,N′*-bis(2-pyridylmethyl)-1,4,7-triazacyclonon-1-yl]-2-propanol (tmpdtnp-OH).** The method outlined previously for the preparation of tmpdtne[1] was employed using either dtn*m*-X·6HBr (6.0 g, 7.1 mmol) or dtnp-OH·6HBr (6.0 g, 7.5 mmol) as starting materials and reacting them with 4 equiv of picolyl chloride hydrochloride. The products were formed as red oils in ca. 95% yield on adjustment of the pH to 14. Due to their hygroscopic nature, only small quantities of the HBr salts could be isolated. These were used in the spectroscopic analysis of the ligands.

**NMR Spectra ($D_2O$, ppm): tmpdtn*m*-*X*·*x*HBr.** $^1$H NMR 2.77 (s, 8H, $PyCH_2NCH_2CH_2NCH_2Py$); 3.18 (m, 8H, $PyCH_2NCH_2CH_2N$-bridge); 3.58 (m, 8H, $PyCH_2NCH_2CH_2N$-bridge); 4.27 (s, 8H, $CH_2$−Py); 4.73 (s, 4H, $CH_2$ in bridge); 7.82 (m, 4H, Ar *CH* in bridge); 7.92 (d, 4H, Ar *CH*); 8.03 (t, 4H, Ar *CH*); 8.61 (t, 4H, Ar *CH*); 8.75 (d, 4H, Ar *CH*). $^{13}$C NMR 46.80, 49.12, 51.36 ($CH_2$ on tacn ring), 55.46 ($CH_2$ attached to pyridyl), 58.40 ($CH_2$ on *m*-xylyl backbone), 131.94, 132.75, 134.23 (*C*H on *m*-xylyl backbone), 131.90 (*C* on *m*-xylyl backbone), 126.36, 127.32, 141.57, 147.25 (*C*H on pyridyl ring), 151.52 (*C* on pyridyl ring).

**tmpdtnp-OH·*x*HBr:** $^1$H NMR 2.77 (m, 4H, $CH_2$CH−OH); 3.27 (m, 8H, $PyCH_2NCH_2CH_2N$-bridge); 3.58 (m, 8H, $PyCH_2NCH_2CH_2N$-bridge), 3.76 (s, 8H, $PyCH_2NCH_2CH_2NCH_2Py$); 3.88 (m, 1H, $CH_2CH$-OH); 4.44 (m, 8H, $CH_2$−Py); 8.03 (t, 4H, Ar *CH*); 8.17 (d, 4H, Ar *CH*); 8.63 (m, 4H, Ar *CH*); 8.77 (d, 4H, Ar *CH*). $^{13}$C NMR 52.12 (br, $CH_2$ on tacn ring), 55.72 ($CH_2$ attached to pyridyl), 57.62 ($CH_2$ on 2-propanol backbone), 61.42 (*C*H(OH) on 2-propanol backbone), 126.35, 127.53, 141.58, 147.16 (*C*H on pyridyl ring), 151.77 (*C* on pyridyl ring).

**[$Cu_2$(tmpdtn*m*-X)]($ClO_4$)$_4$·2DMSO·2$H_2O$ (5).** The method used previously to prepare complex **2**[1] was followed. tmpdtn*m*-X (0.53 g, 0.74 mmol) was dissolved in ethanol (20 mL) and excess $Cu(NO_3)_2$·3$H_2O$ (0.37 g, 1.54 mmol) added, producing a light blue precipitate. The addition of distilled $H_2O$ (10 mL) to this suspension with gentle warming resulted in a dark blue solution. Addition of excess $NaClO_4$ (1 g) to this solution produced a light blue solid which was collected and washed with cold $H_2O$ (yield: 0.36 g, 39%). A dark blue crystalline product was obtained by recrystallization from a DMSO/$H_2O$ mixture.

**Characterization. Anal.** Calcd for [$Cu_2(C_{44}H_{56}N_{10})$]($ClO_4$)$_4$·2DMSO·2$H_2O$: C 40.0, H 4.7, N 11.7, $ClO_4^-$ 31.9, Cu 10.2. Found: C 39.9, H 4.6, N 11.9, $ClO_4^-$ 32.0, Cu 10.3. Electron microprobe: Cl/Cu ratio 2:1. UV−visible spectrum ($CH_3CN$): $\lambda_{max}$, nm ($\epsilon_{max}$, $M^{-1}$) 597 (412), 936 (121). Infrared spectrum (KBr, $cm^{-1}$): 3427s, 2924w, 1613s, 1487m, 1448m, 1384w, 1315w, 1089vs, 1029w, 803w, 769w, 668w, 626s, 418w. Magnetic moment: $\mu_{eff}$ (292 K) = 1.89 $\mu_B$ per Cu(II), variable temperature susceptibility showed no evidence of magnetic coupling.

**[$Cu_2$(tmpdtnp-OH)]($ClO_4$)$_4$ (6).** The method used to prepare complex **5** was followed except that tmpdtnp-OH (2.50 g, 3.69 mmol) and $Cu(NO_3)_2$·3$H_2O$ (1.87 g, 7.75 mmol) were used (yield: 1.55 g, 35%). Recrystallization from a $CH_3CN/H_2O$ mixture gave a dark-blue crystalline product.

**Characterization. Anal.** Calcd for [$Cu_2(C_{39}H_{53}N_{10}OH)$]($ClO_4$)$_4$: C 38.9, H 4.5, N 11.6, $ClO_4^-$ 33.1, Cu 10.6. Found: C 38.7, H 4.4, N 11.5, $ClO_4^-$ 33.2, Cu 10.3. Electron microprobe: Cl/Cu ratio 2:1. ESM spectrum $\{[LM_2](ClO_4)_3\}^+$ 1103.1, $\{[LM_2](ClO_4)_2\}^{2+}$ 502.2, $\{[(L-H)M_2](ClO_4)\}^{2+}$ 452.2. UV−visible spectrum ($CH_3CN$): $\lambda_{max}$, nm ($\epsilon_{max}$, $M^{-1}$) 615 (304), 1017 (83). Infrared Spectrum (Nujol, $cm^{-1}$): 3440s, 1613s, 1573w, 1488m, 1462m, 1377s, 1316w, 1087vs, 971m, 827w, 802w, 769m, 726w, 623s. Magnetic moment: $\mu_{eff}$ (292 K) = 1.78 $\mu_B$ per Cu(II), variable temperature susceptibility showed no evidence of magnetic coupling.

**Crystallography.** Intensity data for a purple prismatic crystal of **3** and a blue prismatic crystal of **4** were measured on a Rigaku AFC6S diffractometer fitted with either graphite-monochromated Cu Kα (**3**) or Mo Kα (**4**) radiation. Cell constants were obtained from a least-squares refinement using the setting angles of 25 reflections ($41.4 < 2\theta < 57.1°$ for **3**), ($22.0 < 2\theta < 28.8°$ for **4**). The data were collected using the $\omega-2\theta$ scan technique. The $2\theta_{max}$ was 120.1 for **3** and 50.1 for **4** with *hkl* values ranging from, respectively, 0 to 16, −15 to 0, and −32 to 32 for **3**; and 0 to 14, −15 to 15, and −16 to 16 for **4**. The intensities of three representative reflections were measured after every 150 reflections. A linear correction factor was applied in the case of **3** to account for an increase in the intensity of the standards by 4.9% over the collection period. The data were corrected for Lorentz and polarization effects[16] and an empirical absorption correction applied case.[17]

The structure of **3** and **4** were solved by heavy-atom Patterson[18a] and direct[18b] methods, respectively, and expanded using Fourier techniques in the DIRDIF94 program.[19] In **4**, a molecule of DMF was refined over two positions. All non-hydrogen atoms were refined with anisotropic thermal parameters in each case, except for the perchlorate oxygen atoms in **3** which were refined isotropically. Hydrogen atoms were included in calculated positions and were not refined. The maximum and minimum peaks on the final difference Fourier map corresponded to 1.07 and −0.49 e $Å^{-3}$ for **3** and to 1.45 and −0.94 e $Å^{-3}$ for **4**. Crystal parameters and details of the data collection and refinement of the structures are summarized in Table 1, selected bond lengths and angles in Table 2, and views of the complexes in Figures 1 and 2.

**Molecular Mechanics Calculations.** Calculations were performed with MOMEC, an empirical force field calculation program which is especially suitable to model coordination complexes containing transition metal ions,[9−11,20] using published force fields.[9−11] Prior to carrying out strain-energy minimizations on complexes **5** and **6**, it became clear that new MOMEC force field parameters needed to be derived to ensure that the best representation of each solution structure was obtained. This was achieved by carrying out calculations on complexes **2**−**4**, since X-ray structural information is available for assessing the agreement between the experimental and predicted structures. A new nitrogen atom type (NTP) was defined to account for the axial elongation, and concomitant changes were made to other force field parameters, viz., bond stretch parameters for CT−NTP ($k_r$ = 6.000 mdyn $Å^{-1}$, $r_0$ = 1.490 Å) and CU2P−NTP (($k_r$ = 0.100 mdyn $Å^{-1}$, $r_0$ = 2.150 Å), torsion parameters for **−CT−NTP−** ($k_\phi$ = 0.0010 mdyn $rad^{-1}$, $m$ = 3, $\phi_{off}$ (rad) 0.000) and angle parameters for CA−CT−NTP, CT−CT−NTP, and CT−NTP−CT ($k_\theta$ = 0.450 mdyn $rad^{-1}$, $\theta_0$ (rad) = 1.911). Calculated structural parameters for **2**−**4** are compared with those from the crystallography in Table 2 which also lists the parameters for **5** and **6**.

**EPR Simulations.** The spin-Hamiltonian parameters, the Cu(II)···Cu(II) separations, and the relative orientations of the two chromophores in the binuclear Cu(II) complexes **1**−**4** were determined by simulation

(15) Rudilph, M.; Reddy, D.; Feldberg, S. W. *Anal. Chem*. **1994**, *66*, 589A.

(16) XDISK *Data Reduction Program*, Version 4.20.2PC, Siemens Analytical X-ray Instruments, Inc.: Madison, WI, 1989.

(17) Walker, N.; Stuart, D. *Acta Crystallogr., Sect. A* **1983**, *39*, 158.

(18) (a) PATTY: Beurskens, P. T.; Admiraal, G.; Beurskens, G.; Bosman, W. P.; Garcia-Granda, S.; Gould, R. O.; Smits, J. M. M.; Smykalla, C. *The DIRDIF Program System*, Technical Report of the Crystallography Laboratory, University of Nijmegen: The Netherlands, 1992. (b) SIR92: Altomare, A.; Cascarano, M.; Giacovazzo, C.; Guagliardi, A. *J. Appl. Crystallogr*. **1993**, *26*, 343.

(19) DIRDIF94: Beurskens, P. T.; Admiraal, G.; Beurskens, G.; Bosman, W. P.; de Gelder, R.; Israel, R.; R. O.; Smits, J. M. M. *The DIRDIF-94 Program System*, Technical Report of the Crystallography Laboratory; University of Nijmegen: The Netherlands, 1994.

(20) Comba, P.; Hambley, T. W., Lauer, G.; Okon, P. MOMEC: *A molecular mechanics program for coordination compounds*, adapted to HyperChem; Lauer & Okon: Heidelberg, Germany; e-mail: CVS−HD@T-ONLINE.de.

**Table 1.** Crystallographic Data for $[Cu_2(tmpdtnp)](ClO_4)_4$ (**3**) and $[Cu_2(tmpdtnb)](ClO_4)_4 \cdot 4DMF$ (**4**)

| | | |
|---|---|---|
| chemical formula | $C_{39}H_{54}Cl_4Cu_2N_{10}O_{16}$ | $C_{52}H_{56}Cl_4Cu_2N_{14}O_{20}$ |
| $f_w$, g mol$^{-1}$ | 1187.82 | 1466.00 |
| crystal dimensions (mm) | 0.36 × 0.18 × 0.16 | 0.36 × 0.16 × 0.12 |
| space group | $P2_1/c$ (No. 14) | $P\bar{1}$ (No. 2) |
| $a$, Å | 13.867(3) | 11.775 (4) |
| $b$, Å | 13.548(6) | 12.738(3) |
| $c$, Å | 28.055(4) | 13.201(3) |
| $\alpha$, deg | | 61.25(2) |
| $\beta$, deg | 102.63(1) | 75.99(3) |
| $\gamma$, deg | | 77.66(3) |
| $V$, Å$^3$ | 5143(2) | 1673(1) |
| $Z$ | 4 | 1 |
| $T$, °C | −60(1) | 23(1) |
| $\lambda$, Å | 1.54178 (Cu Kα) | 0.7107 (Mo Kα) |
| $D_c$, g cm$^{-3}$ | 1.534 | 1.455 |
| $F$(000) | 2448 | 752.0 |
| $\mu$, cm$^{-1}$ | 35.82 (CuKα) | 8.74 (Mo Kα) |
| transmission factor range | 0.8808−1.0000 | 0.9737−1.000 |
| No. of data measured | 8416 | 6250 |
| No. of unique data | 8038 | 5937 |
| No. of observed data ($I \geq 3\sigma(I)$) | 3696 | 3876 |
| No. of parameters refined | 638 | 424 |
| $R^a$ | 0.085 | 0.072 |
| $R_w{}^b$ | 0.089 | 0.065 |
| gof $^c$ | 2.40 | 3.66 |

$^a$ $R(F) = \sum(|F_o| - |F_c|)/\sum|F_o|$. $^b$ $R_w = [\sum w(|F_o| - |F_c|)^2/\sum w|F_o|^2]^{1/2}$, $w = [\sigma^2(F_o)]^{-1}$. $^c$ gof $= ([\sum w(|F_o| - |F_c|)^2/(N_{obervns} - N_{params})]^{1/2})$.

of the $\Delta M_s = 1$ resonances with the computer program DISSIM.[21] The structural parameters depend on the relative orientation of the two $N_5$ chromophores defined by the three angles: $\xi$ is the angle between the $z$ axis of the **g** tensor of one of the copper(II) centers and the Cu−Cu vector, $\tau$ is the angle between the z axes of the two **g** tensors, and $\eta$ is the angle between the $x$ axis of one of the **g** tensors and the projection of the Cu−Cu vector in the corresponding $x,y$ plane; $r$ is the Cu···Cu distance. To determine which minimized structure best represented the cations of **5** and **6** in solution, the experimentally derived frozen solution EPR spectra of each complex were compared to the simulated spectra generated by the DISSIM program from the values of $\xi$, $\tau$, $\eta$, and $r$ obtained from the minimized structures and the appropriate $A$ and $g$ values. EPR data are summarized in Table 3.

## Results and Discussion

**Synthesis and Characterization of Ligands and Copper(II) Complexes.** The *m*-xylyl and 2-propanol bridged bis(pentadentate) ligands, tmpdtn*m*-X and tmpdtnp-OH, were formed by reaction of the corresponding bis(tacn) macrocycles with picolyl chloride at pH 10−11 for 2−3 days. Adjustment of the pH to ∼14 gave red-brown oils of the bis(pentadentate) ligands. The HBr salts of the ligands proved difficult to isolate due to their extremely hygroscopic nature, but sufficient quantities were obtained for the measurement of NMR spectra. In particular, the *J*-modulated $^{13}C$ NMR spectral data of tmpdtn*m*-X·*x*HBr and tmpdtnp-OH·*x*HBr reported in the Experimental Section confirm the formation of the two ligands. The spectra differ only in the signals due to the *m*-xylyl and 2-propanol backbones.

Reaction of tmpdtn*m*-X and tmpdtnp-OH free ligands with an excess of $Cu(NO_3)_2 \cdot 3H_2O$ in EtOH produced light blue solids which on dissolution in water and addition of sodium perchlorate precipitated the perchlorate salts in yields of 35−41%. The low yields probably result from use of unpurified ligand directly in complex synthesis. Recrystallization of the tmpdtn*m*-X complex from a DMSO/$H_2O$ mixture yielded **5**, $[Cu_2(tmpdtnm\text{-}X)](ClO_4)_4 \cdot 2DMSO \cdot 2H_2O$, and the tmpdtnp-OH complex from a $CH_3CN/H_2O$ mixture gave **6**, $[Cu_2(tmpdtnp\text{-}OH)](ClO_4)_4$. The IR spectra of the two complexes show three bands due to the pyridine ring skeletal vibrations (C═N and C═C) in the 1400−1620 cm$^{-1}$ region confirming the presence of the ligand and bands at 1090 and 625 cm$^{-1}$ due to the perchlorate counterions. A characteristic sharp OH stretch is clearly evident at 3440 cm$^{-1}$ when the IR spectrum of the tmpdtnp-OH complex is run in Nujol.

Both the room temperature moments and variable temperature magnetic susceptibility measurements confirmed the absence of magnetic interaction between the two Cu(II) centers. This lack of M···M interaction reflects the large Cu···Cu separations, ≥7.5 Å (see later).

UV−visible spectral data for **5**, **6**, and the previously reported complexes of dmptacn, tmpdtne, tmpdtnp, and tmpdtnb, **1**−**4**, are shown in Table 3. The solution and mull spectra of $[Cu_2(tmpdtnm\text{-}X)]^{4+}$ are similar to that for complexes **2**−**4** showing a strong band at 597 nm that is due to a $d_{xz}$, $d_{yz} \rightarrow d_{x^2-y^2}$ transition[1,13] and a weak, broad band at 936 nm corresponding to a $d_{xy} \rightarrow d_{x^2-y^2}$ transition. For these types of complexes, this is consistent with close to square pyramidal (SP) copper(II) geometry. The UV−visible data, and ES mass spectral data on **6**, further indicate that no dissociation of the complexes occurs in acetonitrile solution and we find no evidence for the formation of mononuclear sandwich complexes such as those observed for bis(tacn) macrocycles.[8,22] This is not surprising since the addition of chelating pyridyl groups would be expected to significantly stabilize the binuclear complexes relative to the mononuclear sandwich complexes. The shift in these bands to 615 and 1017 nm for the solution spectrum of $[Cu_2(tmpdtnp\text{-}OH)]^{4+}$ is suggestive of greater distortion from ideal SP toward trigonal bipyramidal (TBP), as was observed for the mononuclear dmptacn complex.

EPR spectral parameters for complexes **1**−**6**, recorded as frozen DMF solutions at 99 K, are summarized in Table 3 along with those for related complexes. In each case, the parameters, in particular $g_{\|} > g_{\perp}$, are indicative of tetragonally distorted Cu(II) geometries with $d^1_{x^2-y^2}$ ground state, including SP geometry. The significant variation in spectra for complexes **2**−**4** with the length of the alkyl chain, specifically the values of $g_{\|}$ and $A_{\|}$, has previously been attributed to the existence of weak dipole−dipole coupling in the complexes of the ethane and propane bridged ligands (**2** and **3**) which is absent in **4** since the Cu···Cu distance is longer.[1] Notably, the complex of the 2-propanol bridged ligand, **6**, exhibits weak dipole−dipole coupling, as might be anticipated from the length of the alkyl chain. This is not the case for the complex of the *m*-xylyl bridged ligand, **5**, where a longer Cu···Cu distance is predicted by molecular modeling (10.4 Å for **5** versus 8.36 Å for **6**, vide infra). The observed variation in dipolar coupling with Cu···Cu distance is not unexpected since $\Delta H_{dip}$ is dependent on $1/r^3$.[21]

**Crystal Structures.** The dinuclear cation in **4**, $[Cu_2(tmpdtnb)](ClO_4)_4 \cdot 4DMF$, is centrosymmetric and features two pentadentate compartments linked via a butane bridge connecting the N(1) atoms (Figure 1) while in **3**, $[Cu_2(tmpdtnp)](ClO_4)_4$, these are linked by a propane bridge also through N(1) (Figure 2).

A significant difference in the structure of **3** compared to that of **4** and the previously reported structure of $[Cu_2(tmpdtne)](ClO_4)_4$ (**2**) is that the two pentadentate compartments of the

(21) Smith, T. D.; Pilbrow, J. R. *Coord. Chem. Rev.* **1974**, *13*, 173.

(22) Zhang, X.; Hsieh, W.; Margulis, T. N.; Zompa, L. J. *Inorg. Chem.* **1995**, *34*, 2883.

**Table 2.** Selected Bond Distances (Å) and Angles (deg) for $[Cu_2(tmpdtnp)](ClO_4)_4$ (**3**) and $[Cu_2(tmpdtnb)](ClO_4)_4 \cdot 4DMF$ (**4**) and Calculated Parameters for **3**, **4**, $[Cu_2(tmpdtn$*m*$\text{-X})](ClO_4)_4$ (**5**), and$[Cu_2(tmpdtnp\text{-OH})](ClO_4)_4$ (**6**)

| | **2**[a] | **2**[b] | **3**[a] | **3**[b] | **4**[a] | **4**[b] | **5**[b] | **6**[b] |
|---|---|---|---|---|---|---|---|---|
| Cu−N(1) | 2.205(4) | 2.21 | 2.18(1) | 2.25 | 2.242(5) | 2.25 | 2.20 | 2.22 |
| Cu−N(2) | 1.993(4) | 2.02 | 2.02(1) | 2.00 | 2.039(5) | 2.00 | 2.02 | 2.03 |
| Cu−N(3) | 2.009(4) | 2.03 | 2.03(1) | 2.04 | 2.016(5) | 2.02 | 2.03 | 2.02 |
| Cu−N(4) | 1.978(4) | 2.01 | 2.00(1) | 2.01 | 1.992(5) | 2.00 | 2.01 | 2.00 |
| Cu−N(5) | 2.001(4) | 2.00 | 1.96(1) | 2.00 | 2.014(5) | 1.99 | 2.00 | 2.01 |
| Cu′−N(1′) | | | 2.20(1) | 2.25 | | | 2.20 | 2.22 |
| Cu′−N(2′) | | | 2.03(1) | 2.04 | | | 2.02 | 2.03 |
| Cu′−N(3′) | | | 1.97(1) | 2.00 | | | 2.03 | 2.01 |
| Cu′−N(4′) | | | 1.98(1) | 2.00 | | | 2.02 | 2.00 |
| Cu′−N(5′) | | | 1.99(1) | 2.01 | | | 2.00 | 2.02 |
| Cu···Cu′ | 7.481 | 7.47 | 8.087 | 8.49 | 8.68 | 8.41 | 10.40 | 8.36 |
| | | | | | | | | |
| N(1)−Cu-N(2) | 83.8(2) | 85.4 | 84.2(5) | 87.3 | 85.6(2) | 87.5 | 85.1 | 83.9 |
| N(1)−Cu-N(4) | 101.3(2) | 118.2 | 102.5(5) | 98.5 | 95.3(2) | 95.0 | 96.4 | 120.1 |
| N(2)−Cu-N(3) | 85.3(2) | 85.4 | 85.1(6) | 85.4 | 84.9(2) | 85.9 | 85.6 | 85.4 |
| N(2)−Cu-N(5) | 81.1(2) | 82.6 | 160.9(6) | 151.3 | 151.7(2) | 148.2 | 151.7 | 167.9 |
| N(3)−Cu-N(5) | 160.2(2) | 167.8 | 82.1(5) | 83.1 | 83.7(2) | 83.9 | 83.1 | 82.7 |
| N(1)−Cu-N(3) | 85.4(2) | 83.9 | 83.5(4) | 83.6 | 84.0(2) | 85.0 | 84.0 | 85.3 |
| N(1)−Cu-N(5) | 106.7(2) | 97.6 | 108.2(4) | 117.3 | 118.8(2) | 121.7 | 119.2 | 96.9 |
| N(2)−Cu-N(4) | 167.0(2) | 151.6 | 83.6(5) | 82.9 | 83.2(2) | 83.3 | 82.8 | 83.2 |
| N(3)−Cu-N(4) | 83.2(2) | 83.2 | 166.5(5) | 168.1 | 168.1(2) | 169.2 | 168.3 | 151.6 |
| N(4)−Cu-N(5) | 108.3(2) | 106.5 | 106.9(5) | 106.1 | 106.8(2) | 105.1 | 106.6 | 106.5 |
| Energy, kJ mol$^{-1}$ | | 202 | | 201 | | 202 | 211 | 211 |

[a] From X-ray crystal structure. [b] From molecular mechanics calculations.

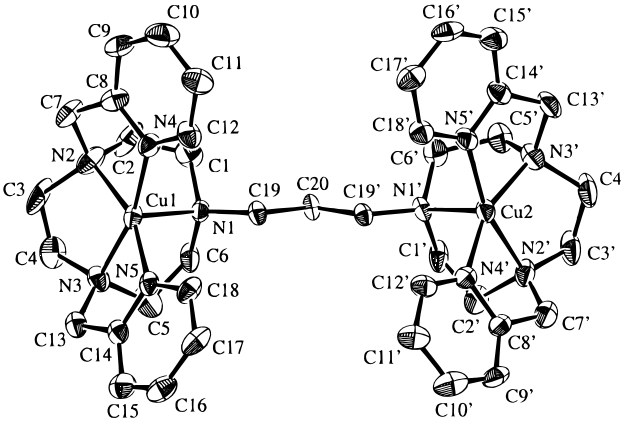


**Figure 1.** Molecular structure and atomic labeling scheme for $[Cu_2(tmpdtnp)](ClO_4)_4$ (**3**). (Thermal ellipsoids are drawn at 20% probability.)

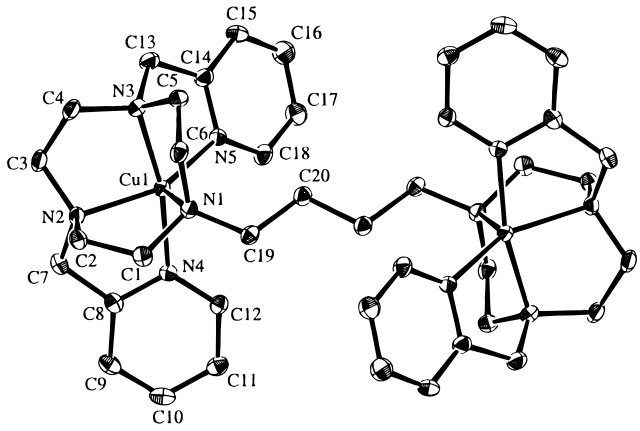


**Figure 2.** Molecular structure and atomic labeling scheme for $[Cu_2(tmpdtnb)](ClO_4)_4 \cdot 4DMF$ (**4**). (thermal ellipsoids are drawn at 20% probability.)

propane bridged complex are oriented toward one another in a syn rather than an anti configuration. Although this may appear electrostatically unfavorable, modeling calculations (see below) indicate little difference in the electrostatic energy term for the two configurations so that the generation of this closed structure is probably governed predominantly by the bridge itself which prefers to orient the $CH_2$ groups in a "zigzag" fashion. This type of geometry was also observed for the corresponding propane bridged bis(tacn) complex, $[Cu_2(dtnp)Cl_4] \cdot 2H_2O$, where the two $Cl^-$ ligands attached to each Cu(II) center were approximately syn to one another.[22] Despite the syn configuration of the tmpdtnp complex, the intramolecular Cu···Cu separation of 8.09 Å in this complex is 0.61 Å longer than that observed in the tmpdtne complex due to the extra carbon atom in the bridge. Notably this distance is significantly shorter than the Cu···Cu distance of 8.6 Å reported for $[Cu_2(dtnp)Cl_4] \cdot 2H_2O$.[22]

The anti orientation of the ligand compartments in **4**, which is similar to that in **2**, is also observed for the corresponding butane bridged bis(tacn) complex, $[Cu_2(dtnb)Cl_4]$, where the two $Cl^-$ ligands attached to each Cu(II) center were approximately anti to one another.[22] As a result of the extra $CH_2$ in the bridge, the intramolecular Cu···Cu separation of 8.68 Å in **4** is 0.59 Å longer than that in the propane bridged complex, **3**. The Cu··· Cu distance is also longer than that for $[Cu_2(dtnb)Cl_4]$ by ca. 0.4 Å.[22]

Each slightly different pentadentate compartment of the ligand in **3** defines a distorted SP geometry about each copper center with the N(1) and N(1′) in the apical position. The Cu−N(1) and Cu′−N(1′) distances (2.18(1) and 2.20(1) Å, respectively) are longer than the Cu−N distances within the equatorial plane formed by two pyridyl and two tacn nitrogens. These distances match those found in **2**. In the corresponding $[Cu_2(dtnp)Cl_4] \cdot 2H_2O$ complex,[22] the Cu−N(1) distance of 2.251(4) Å is 0.071 Å longer than that in **3**. The 2-pyridylmethyl pendant arms appear to prevent the apical bond from lengthening to the extent shown in $[Cu_2(dtnp)Cl_4] \cdot 2H_2O$. In the centrosymmetric complex, **4**, the Cu−N(1) distance (2.242(5) Å) is appreciably longer than the other Cu−N distances and is also longer than the apical bond in **2** and **3**.

In **3**, the two five-membered rings involving the pyridine arms are puckered, viz., Cu/N3/C7/C8 and Cu/N2/C13/C14 torsion

**Table 3.** EPR and UV−Visible Spectral Data for 1-6 Recorded at the X-band Frequency

| | EPR spectra | | | | | UV−Visible spectra |
|---|---|---|---|---|---|---|
| complex | $g_{\|}$[a] | $g_{\perp}$[a] | $A_{\|}$[a] | $A_{\perp}$[a] | solvent | $\lambda_{max}$, nm ($\epsilon_{max}$) |
| **1** $[Cu(dmptacn)](ClO_4)_2$[b,c] | 2.23 | 2.049 | 180 | 10 | $CH_3CN$ | 612 (210); 969 (62); 613(176)[b] |
| | | | | | Nujol mull | 619 br; 600[b] |
| **2** $[Cu_2(tmpdtne)](ClO_4)_4 \cdot 2H_2O$[c] | 2.28 | 2.052 | 126 | 26 | $CH_3CN$ | 598 (398), 924 (118) |
| | | | | | Nujol mull | 602 br |
| **3** $[Cu_2(tmpdtnp)](ClO_4)_4$[c] | 2.30 | 2.055 | 120 | 37 | $CH_3CN$ | 602 (436), 944 (108) |
| | | | | | Nujol mull | 602 br |
| **4** $[Cu_2(tmpdtnb)](ClO_4)_4$[c] | 2.22 | 2.057 | 196 | 10 | $CH_3CN$ | 600 (420), 948 (110) |
| | | | | | Nujol mull | 596 br |
| **5** $[Cu_2(tmpdtnm\text{-}X)](ClO_4)_4$[d] | 2.21 | 2.062 | 185 | 10 | $CH_3CN$ | 597 (412), 936 (121) |
| | | | | | Nujol mull | 600 br |
| **6** $[Cu_2(tmpdtnp\text{-}OH)](ClO_4)_4$[d] | 2.31 | 2.070 | 120 | 37 | $CH_3CN$ | 615 (304), 1017 (83) |
| | | | | | Nujol mull | 600 br |

[a] Recorded at the X-band frequency, $A$ values are $\times 10^{-4}$ $cm^{-1}$. [b] Reference 13. [c] Reference 1. [d] This work.

angles are 39(1)° and −40(1)°, respectively as previously observed for **1**. The degree of distortion of the Cu(II) geometry from SP toward TBP for **3** (9%) is similar to that found for **2** (11%) and less than that for **1** (32%). Complex **4** shows a similar degree of distortion from SP (27%) to **1**. The basal plane of the distorted SP geometry observed in **4** is defined by the atoms N(2), N(3), N(4), and N(5). The Cu atom lies 0.26 Å out of this plane toward the N(1) atom. This distortion is greater than that observed in **2** where the Cu atom is situated 0.19 Å above the basal plane but less than that seen in **1** where the Cu atom lies 0.32 Å above the plane. Unlike in the case of **1** and **3**, the two five-membered rings involving the pyridine rings are close to planar in **4** (as in **2**), viz., the Cu/N(4)/C(8)/C(7) and Cu/N(5)/C(14)/C(13) torsion angles are 6.8(7) and −2.9(6)°, respectively.

**Molecular Modeling Calculations.** Despite numerous attempts, single crystals of $[Cu_2(tmpdtnm\text{-}X)](ClO_4)_4$ (**5**) and $[Cu_2(tmpdtnp\text{-}OH)](ClO_4)_4$ (**6**) suitable for X-ray crystallography could not be obtained. Hence, molecular mechanics was utilized in conjunction with EPR simulation to predict the preferred solution structures of these complexes.[9−11]

Structural parameters obtained from molecular mechanics calculations of complexes **2**−**4** compare well with X-ray structural data for these complexes (Table 2). In each case, there is a good match in the coordination environment about each copper center with differences in Cu−N distances of ≤0.04 Å and in N−Cu−N angles of ≤4°. In general, the agreement was at the lower end of these limits. We note, however, that in the case of complex **2**, the deviation in one of the calculated trans angles was higher (17°); in the case of complex **3**, one apical bond was 0.07 Å longer in the calculated structure and the calculated N(2)−Cu−N(5) angle was 10° smaller than the observed. The calculated Cu···Cu distance in **2** is in excellent agreement with that observed in the crystal structure. Some interesting differences were observed for complexes **3** and **4**. The calculated Cu···Cu distance for **3** of 8.49 Å is 0.40 Å longer than that obtained from crystallography, while in the case of **4**, the calculated value of 8.41 Å is 0.27 Å shorter than in the X-ray structure. These differences could be due to distortions of the optimum solution phase structures by crystal packing effects. Notably, the calculated Cu···Cu distance for **4** is in good agreement with that observed in $[Cu_2(dtnb)Cl_4]$ (8.3 Å).[22] Electrostatic interactions between the Cu(II) centers have been modeled for these complexes to see if there was a significant difference for the syn and anti configurations. Such differences were small (≤2kJ $mol^{-1}$) for complexes **3**−**6** where the Cu···Cu separations are ≥∼8.0 Å. For **2**, however, the electrostatic interaction energy is ∼10 kJ $mol^{-1}$ greater for the syn when compared with the anti configuration due to a much shorter Cu···Cu distance (viz., ∼ 6.2 Å for syn and 7.5 Å for anti).

Calculations on complexes **5** and **6** were undertaken on a range of different conformers (15−20) for each complex. Following these MOMEC calculations, a number of conformers could be discounted as possible solution structures for complexes **5** and **6** because the total strain energies were comparatively high in relation to the other conformers. However, it became evident that, for each complex, groups of conformers with anti and syn configurations were most stable and had very similar total strain energy, a finding which indicates that complexes with either configuration can be formed by such ligands. For the Cu(II) complexes of dtne bearing four alcohol pendant arms, the anti configuration is preferred when the alcohol groups are coordinated to the metal center.[4] Partial deprotonation, however, leads to stabilization of the syn configuration through a reduction in electrostatic repulsion and H-bonding between pairs of protonated and deprotonated alcohol groups.[4] Thus, for octahedral metal centers, stabilization of the syn configuration could be envisaged through the introduction of exogenous and/or endogenous bridging groups. The ability to "lock in" a particular conformation is akin to the conformational changes that can occur when a substrate attaches to, for example, a polynuclear biosite.

The calculated structural parameters ($\xi$, $\tau$, $\eta$, and $r$) obtained from the minimized structures for **5** and **6** were used in the simulation of the EPR spectra. The $A$ and $g$ values were varied until the best fit was achieved. The plots shown in Figure 3 depict the experimental and simulated EPR spectra of the syn and anti configurations of $[Cu_2(tmpdtnm\text{-}X)](ClO_4)_4$ (**5**) together with the structural parameters. The spectrum simulated on the basis of the structural parameters for the anti configuration of **5** better matches the experimental signal intensity than that simulated using parameters for the syn configuration. However, since the mimimized strain energy for the two configurations are very similar, viz., the anti configuration with the lowest strain energy is only ca. 3.5 kJ $mol^{-1}$ more stable than the corresponding syn configuration, it is likely that both of these configurations are present in solution and that this is reflected in the observed EPR spectrum. A similar conclusion is reached for the syn and anti configurations of **6** where the strain energies for the syn and anti configurations are essentially identical.

In comparing the structures of **5** and **6** with those of **1**−**4**, we focus on the lowest energy conformations of **5** and **6**. The predicted solution structures of **5** and **6** (Figure 4, parts a and b) show that the two pentadentate compartments define a

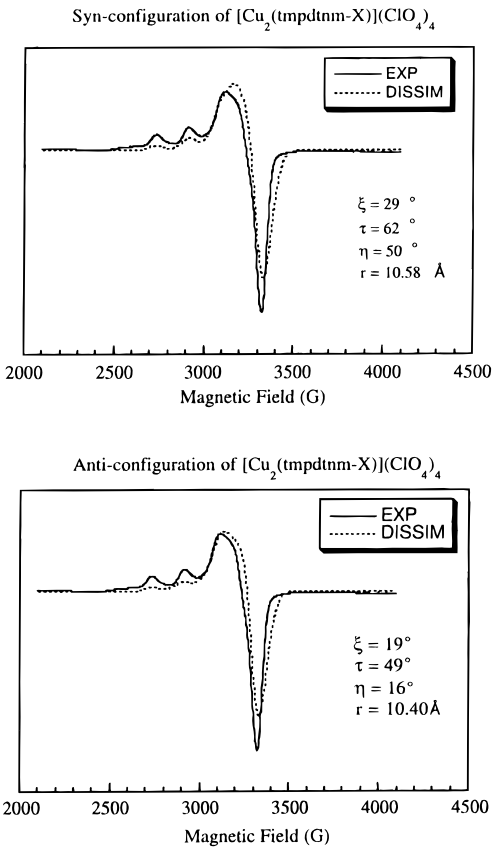


**Figure 3.** Experimental and simulated spectra of the syn and anti configurations of **5**.

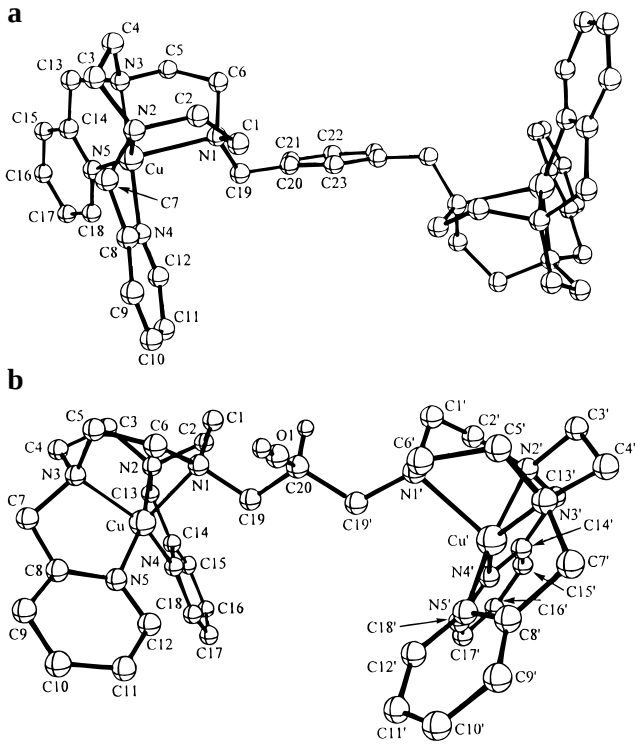


**Figure 4.** Molecular structures of the (a) anti configuration of **5** (b) and the syn configuration of **6**.

distorted SP geometry about each Cu(II) center. In **5**, the Cu···Cu separation in the anti form is quite large (10.40 Å), as might be expected from the orientation of the aromatic bridge, while in **6**, this separation is 8.36 Å. The latter is 0.27 Å longer than that found in **3** which also has a three-carbon chain linking the ligand compartments. A widening of the angle between the three bridging carbon atoms [C(19)−C(20)−C(19′)] to 111° compared to 105° in **3** contributes to this. As found for complexes **1**−**4**, the apical Cu−N(1) bond (2.20 Å in **5** and 2.22 Å in **6**) is elongated compared to the other Cu−N distances. The puckered nature of the two five-membered rings involving the pyridine arms in **1** and **3** is also evident in **5** and **6** (for **5**, the Cu−N(3)−C(13)−C(14) and Cu−N(2)−C(7)−C(8) torsion angles are 34.2 and 38.3°, respectively, while for **6**, the Cu−N(3)−C(7)−C(8) and Cu−N(2)−C(13)−C(14) torsion angles are 37.9 and 31.5°, respectively. Significant distortion of the geometry from SP toward TBP is found in **5** (28%) and **6** (30%) which is comparable to that in **4** and **1**.

**Electrochemical Behavior of Complexes 1−6.** The redox behavior of the Cu(II) complexes, **1**−**6**, in acetonitrile has been studied using cyclic voltammetry, square-wave voltammetry, steady-state voltammetry and bulk electrolysis. The voltammetric data are summarized in Table 4. Cyclic voltammograms for **1**, **2**, and **6** (scan rate = 100 mV $s^{-1}$) are displayed in Figure 5, with ferrocene as an internal standard.

In the case of **1**, a small degree of chemical irreversibility is observed in the cyclic voltammogram at low scan rates which is evidenced by the slightly different wave shape and ratio of $i_p^{ox}/i_p^{red}$ relative to that of ferrocene (Figure 5) which is known to be reversibly oxidized. However, since the $E_{1/2}$ value (−0.81 V vs $F_c/F_c^+$) calculated from the average of the oxidation and reduction peak potentials is almost consistent over the scan rate range 10 to 1000 mV $s^{-1}$, we believe it to be a good approximation of the formal (reversible) potential $E_f°$ for the one-electron process (eq 1).

$$\mathrm{Cu(II)} + e^- \rightleftharpoons \mathrm{Cu(I)} \qquad (1)$$

Further supporting this are the $E_{1/2}$ ($E_p$) values, measured via square-wave and steady-state techniques, which are also −0.81 V vs $F_c/F_c^+$ (Table 4).

The binuclear complexes, **2**−**4**, (see CV trace for **2** in Figure 5) all exhibit chemically reversible waves with $E_{1/2}$ values of −0.71 V, −0.72 V, and −0.74 V, respectively, as determined by all three techniques (Table 4). The reversibility is highlighted by the $i_p^{ox}/i_p^{red}$ ratios for **1**−**4** which are all close to unity over the scan rate range of 20−1000 mV $s^{-1}$. Although the $\Delta E_p$ values for **2**−**4**, 56−66 mV, suggest that a one-electron process is taking place, the height of the waves, i.e., the $i_p^{ox}$ and $i_p^{red}$ values, for **2**−**4** (av 5.86−6.57 $\mu$A) are almost double those of the mononuclear complex **1** (3.21−3.69 $\mu$A) which unambiguously corresponds to a one-electron reduction of Cu(II) to Cu(I). However, care must be exercised in attempting to relate peak heights to n, the number of electrons passed, since according to the Randles-Sevcik theory[23] for a reversible process in linear sweep voltammetry, $I_p$ is dependent on $D^{1/2}$, where $D$ is the diffusion coefficient, and also on $n^{3/2}$. Since the binuclear complexes have considerably larger molecular weights, they are likely to diffuse more slowly than the monomeric complex, **1**. Consequently, additional information in the form of square-wave and steady-state voltammetric data was used to confirm that the binuclear complexes, **2**−**4**, undergo a two-electron process at the same (or very similar) potentials.

From the parameters obtained for the three electrochemical techniques, it is possible to verify that $n = 2$ for **2**−**4** because the dependence of peak currents on $n$ and $D$ differ, viz., $I_p \propto D^{1/2}$ and $n^{3/2}$ for cyclic voltammetry,[23] $I_p \propto D^{1/2}$ and $n$ for square-

(23) Bard, A. J.; Faulkner, L. R. *Electrochemical Methods*; John Wiley & Sons: Canada, 1980.

**Table 4.** Cyclic, Square-Wave and Near Steady-State Voltammetric Data Measured for Complexes **1**−**6** in Acetonitrile (0.1 M $Bu_tNClO_4$)[a]

| | cyclic[b] | | | | | | | square−wave[c] | | | near steady-state[d] | | | |
|---|---|---|---|---|---|---|---|---|---|---|---|---|---|---|
| | $E_{1/2}$ (V) | $\Delta E$ (mV) | $E_p^{ox}$ (V) | $E_p^{red}$ (V) | $i_p^{ox}$ ($\mu$A) | $i_p^{red}$ ($\mu$A) | $i_p^{ox}/i_p^{red}$ | $E_p$ (V) | $W_{1/2}$[f] (V) | $I_p$ ($\mu$A) | $E_{1/2}$ (V) | $E_{1/4}-E_{3/4}$[i] (mV) | $I_d$ (nA) | $10^6D$ ($cm^2\,s^{-1}$) |
| $F_c$ | 0.00 | 58 | +0.03 | −0.03 | 4.39 | 4.48 | 1.0 | 0.00 | 0.10 | 11.1 | 0.00 | 58 | 2.07 | 23 |
| 1 | −0.81 | 70 | −0.84 | −0.77 | 3.21 | 3.69 | 0.85 | −0.81 | 0.11 | 8.7 | −0.81 | 61 | 1.24 | 13.3 |
| **2** | −0.71 | 56 | −0.74 | −0.68 | 6.31 | 6.91 | 0.90 | −0.71 | 0.08 | 18.3 | −0.71 | 52 | 1.62 | 7.30 |
| 3 | −0.72 | 58 | −0.74 | −0.69 | 5.47 | 6.23 | 0.90 | −0.72 | 0.09 | 13.2 | −0.72 | 52 | 1.52 | 6.74 |
| 4 | −0.74 | 66 | −0.77 | −0.71 | 5.81 | 6.56 | 0.90 | −0.74 | 0.10 | 12.6 | −0.74 | 52 | 1.64 | 7.51 |
| 5 | −0.73 | 92 | −0.78 | −0.68 | 4.26 | 5.43 | 0.80 | −0.73 | 0.09 | 12.6 | −0.73 | 56 | 1.14 | 5.66[j] |
| 6 | −0.80[e] | 122[e] | −0.86[e] | −0.74[e] | 3.48[e] | 4.22[e] | 0.90[e] | −0.75[g]<br>−0.82[g] | 0.21[h] | 5.8sh[g]<br>7.0[g] | −0.80 | 91 | 1.67 | 8.12[j] |

[a] Potentials are quoted with respect to the $F_c/F_c^+$ couple used as an internal reference. The concentrations of the complexes used were in the range 0.5−0.55 mM, but the current data in the table are normalized to 0.5 mM to facilitate comparison of values. [b] Cyclic voltammetric data were measured at a scan rate of 100 mV $s^{-1}$. [c] Square-wave voltammetric data were measured with a period of 30 ms. [d] Steady-state voltammetric data were measured on a 5-$\mu$m radius Pt microdisk electrode. [e] Average of partially resolved processes (see text). [f] Width at half peak height. [g] Data reported for individual processes. [h] Data reported for combined processes. [i] $E_{1/4}$ and $E_{3/4}$ are the potentials at $^1/_4$ and $^3/_4$ of the total wave height, respectively. [j] Average of unresolved processes.

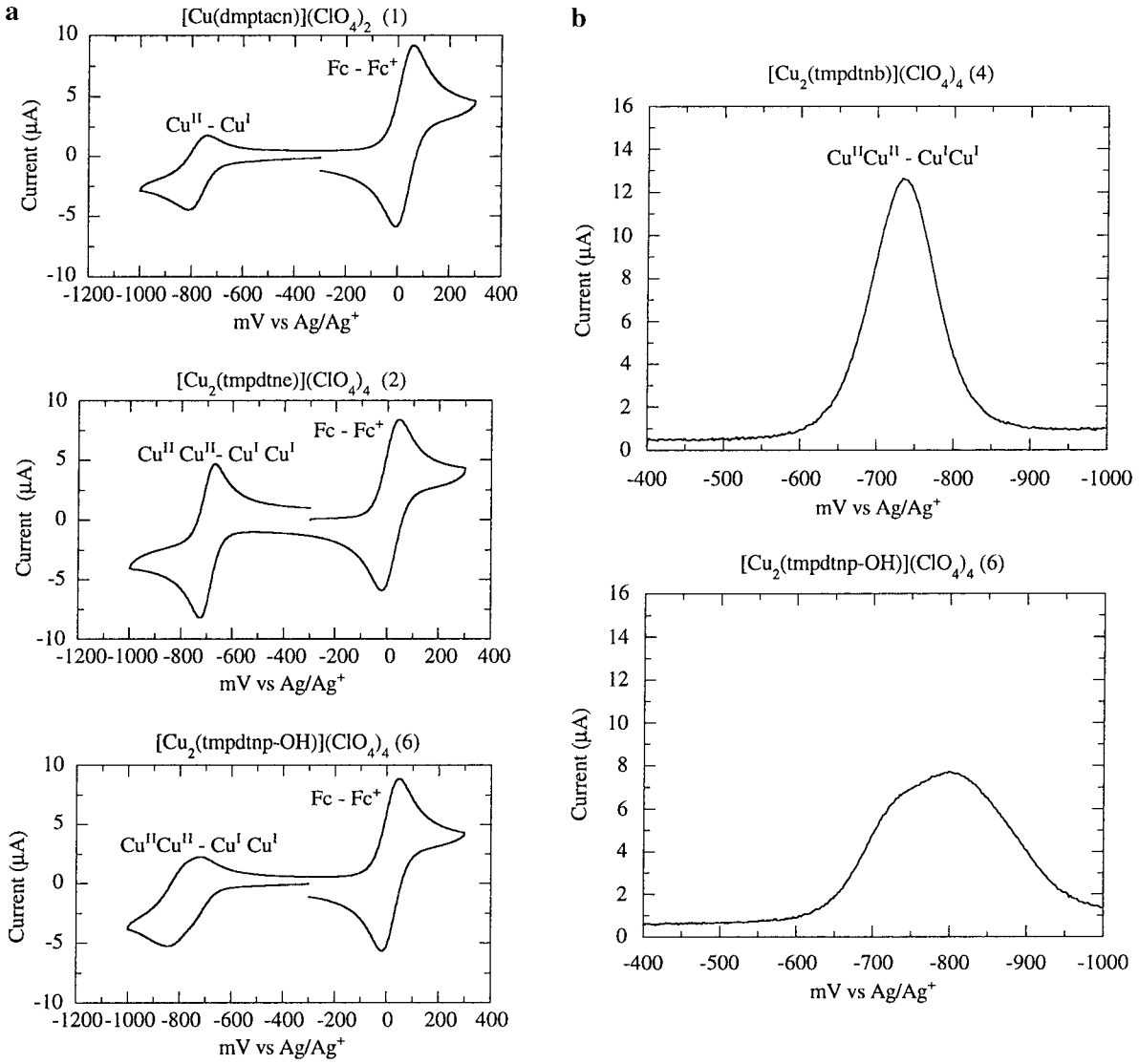


**Figure 5.** (a) Cyclic voltammograms of complexes **1**, **2**, and **6** and (b) square-wave voltammograms of complexes **4** and **6** obtained at a platinum disk electrode ($r = 0.08$ cm) in acetonitrile (0.1 M $Bu_4NClO_4$) at 20 °C.

wave voltammetry[24] and $I_p \propto D$ and $n$ for steady-state voltammetry.[25] Assuming that $n = 1$ for complex **1** and $n = 2$ for complexes **2**−**4**, $D$ was calculated to give the values in Table 4. As anticipated, the diffusion coefficient for **1** is found to be considerably higher than that of the other complexes (ca. double on average). In this circumstance, if $n$ were 1.0 and not 2.0 for the binuclear complexes **2**−**4**, then the peak current values under cyclic or square-wave voltammetric conditions would be smaller than for **1** where $n$ is known to be 1.0. The fact that the peak

(24) Osteryoung, J.; O'dea, J. J. *Electroanal. Chem.* **1986**, *14*, 209.
(25) Bond, A. M.; Oldham, K. B.; Zoski, C. G. *Anal. Chim. Acta* **1989**, *216*, 177.

currents for **2**−**4** are higher than **1** in cyclic voltammetry is a consequence of the power indices of the $n$ and $D$ terms. Thus, in cyclic voltammetry, the peak current ratio for **2**−**4** ($I_{2-4}$) versus that for compound **1** ($I_1$) for a given set of conditions is as predicted if $n = 1$ for **1** and $n = 2$ for **2**−**4** (ie., $I_{2-4}/I_1 = (n_{2-4}/n_1)^{3/2}(D_{2-4}/D_1)^{1/2} = (2/1)^{3/2}(1/2)^{1/2} = 2$). Analogous considerations apply for square-wave techniques since $I_{2-4}/I_1 = (n_{2-4}/n_1)(D_{2-4}/D_1)^{1/2} = (2/1)(1/2)^{1/2} = 1.4$. This latter prediction is closely met for compounds **3** and **4**, but for **2** the experimentally found ratio is larger than predicted. The sensitivity of peak currents in square-wave voltammetry to kinetic nuances could give rise to such a discrepancy. The situations with regard to compounds **5** and **6** are special**.** For **5**, significant chemical irreversibility is observed ($i_p^{ox}/i_p^{red} = 0.80$) so that the normal theoretical treatment does not apply, while for **6**, the very much smaller current is attributable to two partially resolved processes presumably each with $n = 1$. The values of peak currents observed for the cyclic and square-wave techniques reflect this.

Voltammograms for compounds **2**−**4** can be simulated under the assumption that two unresolved reversible processes are present with $n = 1$ and $E_f^\circ$ separated ≤20 mV, a result expected for two weakly or noninteracting copper centers. The voltammogram for **6** can be simulated assuming a small degree of communication occurs between the two copper centers giving rise to a $E_f^\circ$ separation of about 80 mV. Some interaction between the OH group in the 2-propanol bridge and one Cu(II) center could make its reduction more difficult. A number of approaches were used to simulate the voltammetry for compound **5**, but a unique solution was not found. This is because while the $\Delta E_p$ value under cyclic voltammetry conditions is larger than expected for a two-electron reduction at the same potential, the shape of the reverse oxidation process and the peak current data for the reduction and oxidation components implies the presence of a small degree of irreversibility. In contrast, the shapes of the square-wave and steady-state responses are much like that for compounds **2**−**4**. A plausible interpretation is that this compound does not exhibit a purely EE mechanism[23] in which the $E_f^\circ$ value for the second process is assumed to be slightly more negative than $E_f^\circ$ for the first process because a chemical step occurs on the voltammetric time scale after the transfer of either the first or second electron. Unfortunately, under conditions of bulk electrolysis, the Cu(I)-Cu(I) complexes are unstable so that the necessary characterization of the reduced forms of the compounds could not be achieved.

In summary, the voltammetric data suggest that the reduction of **2**−**5** involves two very closely spaced unresolved one-electron processes represented by

$$\mathrm{Cu(II)Cu(II)} + e^- \rightleftharpoons \mathrm{Cu(II)Cu(I)} + e^- \rightleftharpoons \mathrm{Cu(I)Cu(I)}$$

The fact that the reduction of **1** occurs at an $E_{1/2}$ potential, −0.81 V, than the more negative binuclear complexes **2**−**5** (−0.71 V to −0.74 V) indicates that, relative to the Cu(II) state, the reduced Cu(I)Cu(I) forms of the binuclear complexes are more stable than the mononuclear analogue. The data indicate that the effect is dependent on the Cu···Cu separation which in these systems varies with the length of the alkyl chain linking the two ligand compartments and may thus be reflecting electrostatic effects in the Cu(II) state. In keeping with this proposal, the complex of the tmpdtne ligand, **2**, is easiest to reduce since the Cu···Cu separation is shortest and hence repulsion between the positively charged Cu(II) centers is greatest.

## Conclusion

X-ray structural data and molecular modeling studies have revealed interesting variations in the preferred configuration of Cu(II) complexes of a series of bis(pentadentate) ligands with the type and length of the spacer linking the pentadentate ligand compartments. Electrochemical studies also showed that the reduction potentials vary systematically with Cu···Cu separation. That is, reduction becomes more difficult as the separation increases due to stabilization of the Cu(II) state. The chemical reversibility of the voltammetric processes, even though some structural rearrangement may occur in the Cu(I) state, suggests that an electrochemical examination of the potentially significant dioxygen chemistry of the Cu(I) complexes could be warranted.

**Acknowledgment.** This work was supported by the Australian Research Council (L.S. and A.M.B.), the Deutsche Forschungsgemeinschaft (P.C.), and travel grants from Monash University and the Deutscher Akademischer Austauschdienst. S.J.B. was the recipient of a Monash Graduate Scholarship.

**Supporting Information Available:** Listings of atomic coordinates, anisotropic displacement parameters, H atom parameters, all bond distances and angles, torsion angles, and nonbonded contacts (47 pages). Ordering information is given on any current masthead page.

IC971634I